THE IMPACT BEHAVIOR OF COMPOSITES AND SANDWICH STRUCTURES

W.J. Cantwell[a,b*] and Z.W. Guan[a]

[a]*School of Engineering, University of Liverpool, Liverpool, L69 3GH.U.K.*
[b]*Aerospace Research and Innovation Center (ARIC), Khalifa University of Science, Technology and Research (KUSTAR), Abu Dhabi, UAE.*
**cantwell@liv.ac.uk*

Keywords: Impact; Damage; Energy absorption; Sandwich Structures

Abstract

For many years there has been considerable concern regarding the response of composite materials and lightweight sandwich structures to localized impact loading. Extensive testing has shown that very low impact energies are capable of generating significant damage over a large region. The first part of this paper reviews some of the key studies in this area, focusing primarily on experimental attempts to characterize damage initiation and propagation in these structures. The second section of this paper reviews the attempts to use numerical techniques to model the impact response of composites and sandwich structures.

1. Experimental Investigations

Localised impact loading on a composite structure is likely to result in the introduction of significant damage extending both through the thickness of the laminate as well as to locations well beyond the point of contact. Figure 1 shows photographic images of two GFRP panels subjected to impact energies of 0.5 Joules and 3 Joules [1]. From the figures, it is clear that even very low levels of energy can generate sizeable damage zones. Cross-sections of the damage highlight the presence of zones of delamination at many ply interfaces, linked by a complex system of matrix cracks.

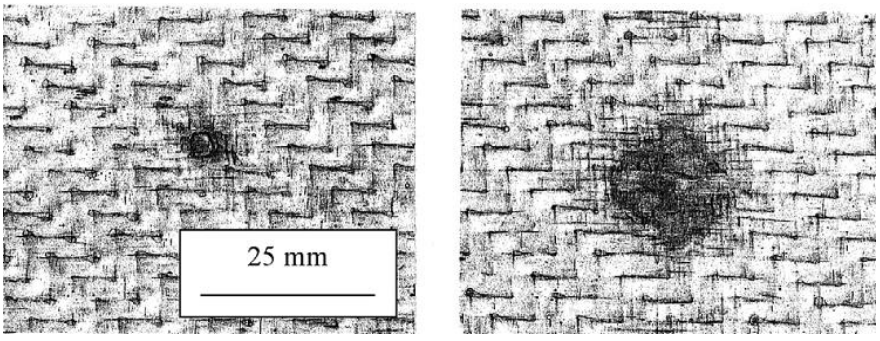

Figure 1. Impact damage in 2.5 mm thick GFRP laminates (i) impact energy = 0.5 Joules, impact force = 866 Newtons (ii) impact energy = 3 Joules,impact force = 2118 Newtons [1].

A very significant threshold is the energy required to initiate damage in a composite structure. Several investigators have used simple models to predict the initiation of impact damage in high-performance composite materials [2-6]. Sjoblom [2] showed that the impact force necessary to initiate damage increases with $t^{3/2}$ where t is the thickness of the laminate Figure 2 show a plot of P_{crit} versus $t^{3/2}$ for a range of glass fibre reinforced epoxy plates. Here, the unsupported diameter was varied between 50 mm and 200 mm. The evidence suggests that, in spite of the fact that there is a significant change in geometry, the data all appear to follow a $t^{3/2}$ dependency.

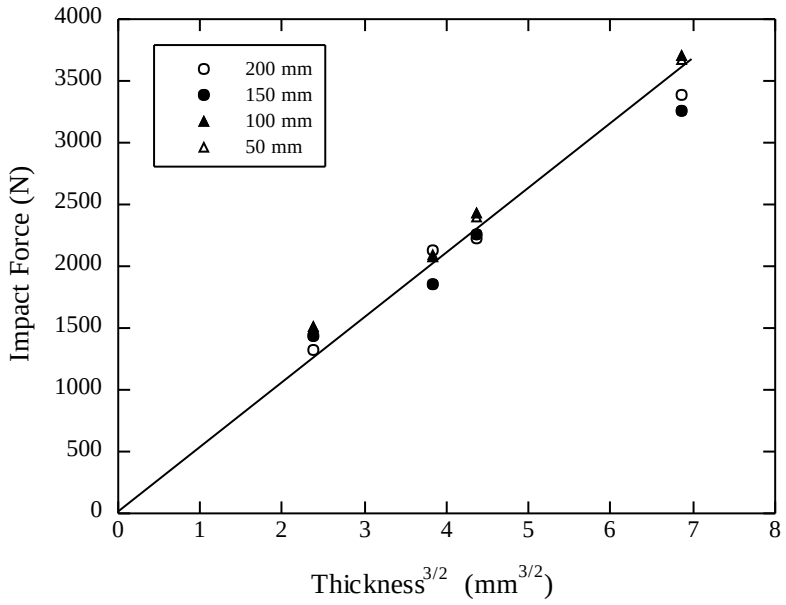

Figure 2. The variation of the damage initiation force with $t^{3/2}$, where t is the specimen thickness. The figure includes data for four support diameters. The impactor diameter was 10 mm [7].

Schoeppner and Abrate [6] used data from a large number tests on several types of composite and found that delamination was associated with a rapid drop in load during the impact event. They showed that the force required to initiate damage also exhibited a $t^{3/2}$ dependency. Following impact tests on a carbon fibre/epoxy, Davies and Zhang [5] suggested that the critical impact force, Pcrit depended on the Mode II interlaminar fracture toughness, G_{IIc}, according to:

$$P_{crit}^2 = \frac{8\pi^2 E t^3 G_{IIc}}{9(1-\nu^2)} \tag{1}$$

Where ν is the Poisson's ratio and E is the in-plane modulus. Here again, the relationship predicts a $t^{3/2}$ dependency for the damage threshold force. It is also interesting to note that the critical force is not sensitive to the planar dimensions of the laminate. Sutherland and Guedes Soares [3] proposed a simple delamination model to predict the onset of failure in marine materials, where it was shown that P_{crii} given by:

$$P_{crit}^2 = \left(\frac{6 \text{ILSS}^3 \pi^3 t^3}{E} \right) R \tag{2}$$

where ILSS is the interlaminar shear strength of the composite and R is the radius of the impactor. It is interesting to note that Equation 2 accounts for changes in projectile diameter, whereas Equation 1 does not. Yang [7] investigated the general applicability of these two models to a glass fibre/epoxy by varying the radius of the steel impactor. It was shown that P_{crit} is dependent on R, suggesting that Equation 2 more generally valid for predicting the onset of impact damage. Following tests on a wide range of structures used a number of values of R, Yang plotted the square of the critical load against $6\pi^3t^3R/E$, Figure 3, and used the slope of the trace to determine the value of ILSS. It was shown that the resulting value was very similar to that measured directly following an impact test on an ILSS specimen [7].

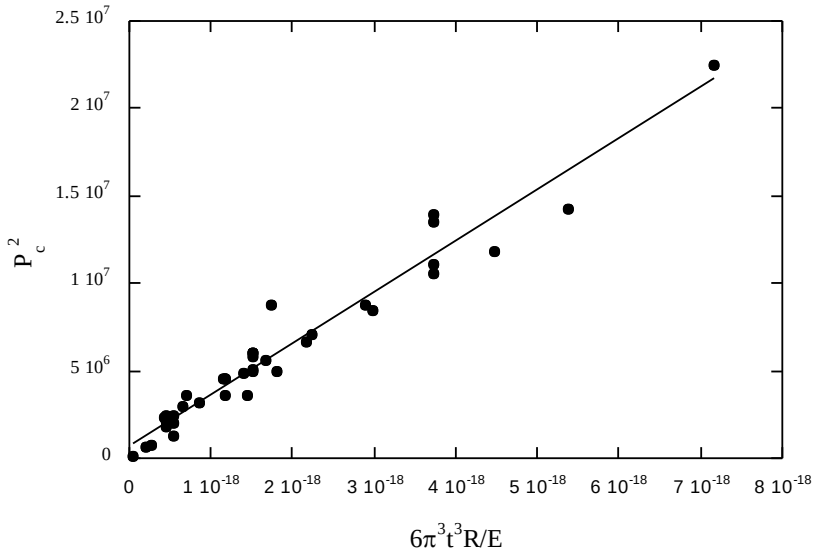

Figure 3. Plot of the square of the critical force, P_c^2, against the parameter $6\pi^3t^3R/E$ for all of the experimental data (indentor diameters, plate diameters) at room temperature [7].

Several researchers have employed damage–force maps to investigate failure in impact-loaded laminates [8.9]. Cantwell conducted impact tests on a GFRP laminate and measured the variation of damage size with impact force, Figure 4 [1]. Here, the impact data for the range of plate diameters investigated in this study appear to fall within a relatively narrow band. The critical force for damage initiation for these samples appear to be similar, lying between 600 and 800 Newtons. The findings in this figure support the findings of Davies and co-workers and Zhou [8,9] who argued that maps of this type are useful for studying damage development in composites.

Research studies have also attempted to study the mechanisms of damage development in sandwich structures [10]. Figure 5 shows cross-sections of two sandwich structures following perforation by a steel projectile. The PVC foam, Figure 5a exhibits a clear cylindrically-shaped perforation zone with dimensions similar to those of the impactor, suggesting that the foam fails in shear. There is also a small conical-shaped crack is in evidence at the exit surface, due to locally-high tensile stresses close to the rear surface. Figure 5b shows the cross-section of a PET-based sandwich structure, where both shear and tensile failure modes are apparent.

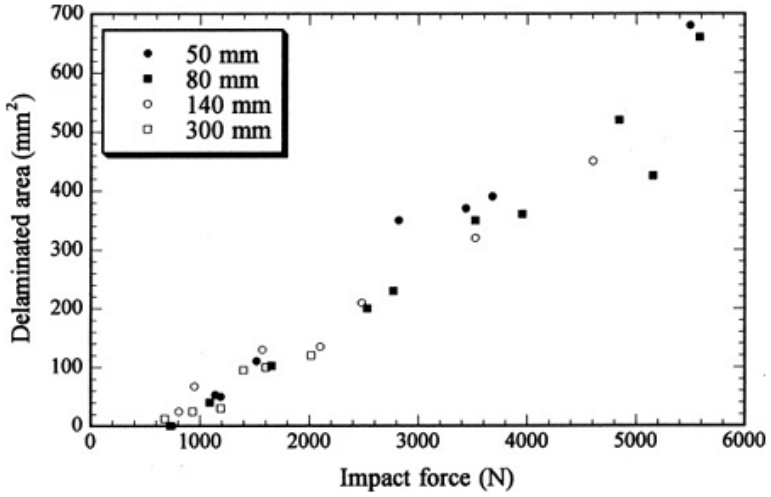

Figure 4. The variation of delaminated area with impact force for a range of samples supported on circular rings [1].

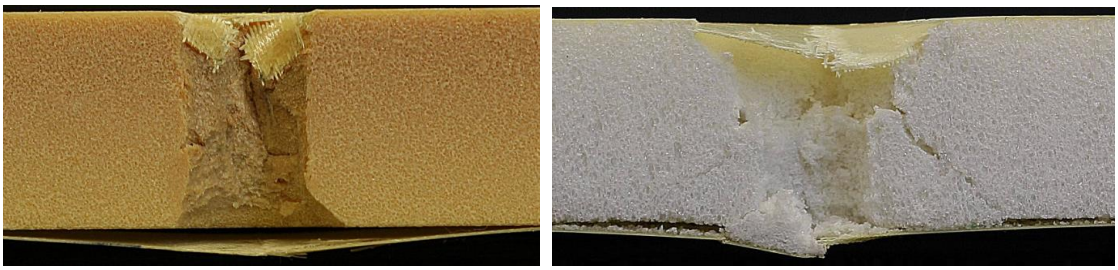

(a) (b)

Figure 5. Cross-sections of the perforated sandwich panels: (a) Crosslinked PVC. (200 kg/m^3), (b) PET. (105 kg/m^3) [10].

Low velocity impact testing on a range of sandwich structures highlighted the influence of the properties of the core material on the fracture behaviour of the top surface skin. It was argued that the critical force depended on the support from the foam. Fatt and Park [11] studied the processes of damage initiation in impact-loaded sandwich panels and showed that the critical impact force for fracture in the skin of a sandwich panel is:

$$F_s = dA_{11}\varepsilon_{crd}(2\varepsilon_{crd})^{0.5} + K_c\pi q_d R_e^{\ 2} \quad (3)$$

Where q_d is the dynamic crushing strength of the foam, ε_{crd} is the dynamic tensile fracture strain, K_c d is the length of damage, A_{11} is the laminate extensional stiffness, is a constraint factor for core crushing and R_e is the effective radius of the projectile This suggests that the critical force increases with the compressive strength of the foam. Figure 6 shows the force required to fracture the upper skin as a function of the properties of the foam. Included in the figure is the force required to fail the uppermost skin peak of two spaced skins (i.e. no core), From the figure, it is clear that the critical force tends to increase with the plastic collapse stress of the foam, suggesting that the Fatt and Park model is capable of predicting the experimental data, highlighting the importance of the properties of the core in the damage initiation process [10].

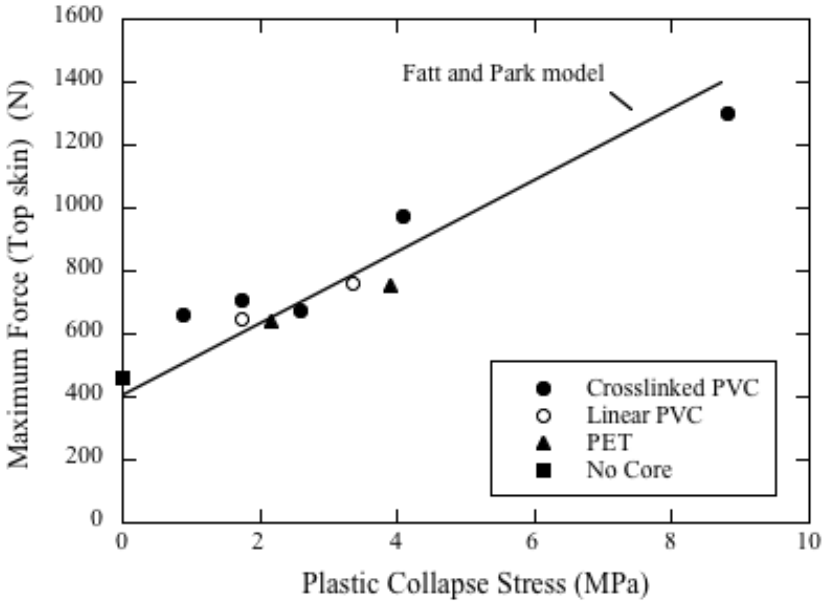

Figure 6. The variation of the force required to fracture the top skin as a function of the plastic collapse stress of the foam core [10].

Research has also shown that the perforation resistance of a foam-based sandwich structure is strongly dependent on the shear fracture properties of the core. Figure 7 shows that variation of the perforation resistance of a sandwich structure as a function of the Mode II work of fracture properties of the associated core material [10]. The Mode II properties were measured on a simple shear specimen at quasi-static rates of loading. Included in Figure 7 is the value corresponding to perforation tests on a sandwich structure without an inner core. Here, a unique relationship exists between the perforation resistance of panels and the Mode II properties of the core [10].

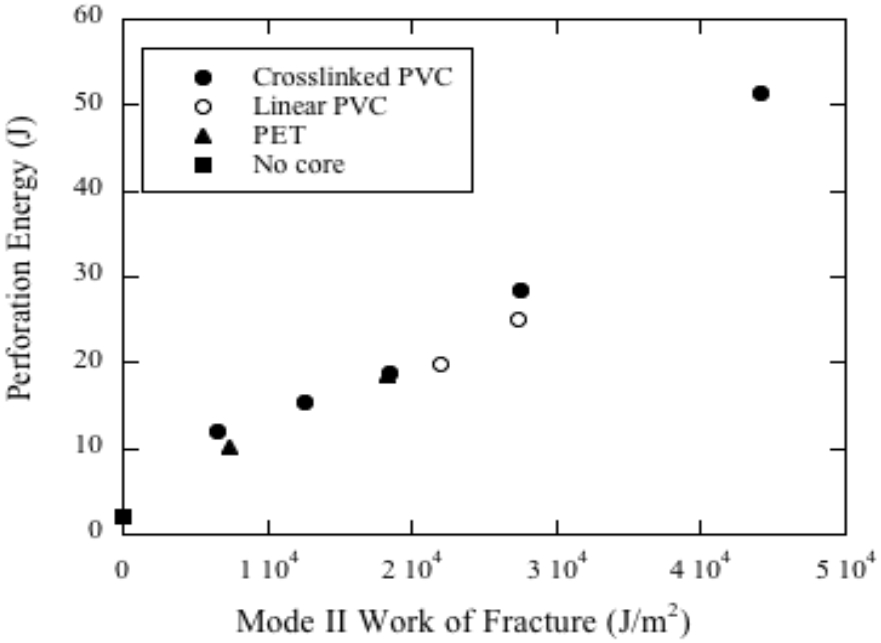

Figure 7. The variation of the perforation energy of the sandwich structure as a function of the Mode II (shear) work of fracture.

2. Numerical modeling

Finite element models have developed to simulate the impact response of composite and sandwich structures including glass fibre reinforced composites and PVC foam-based sandwich panels. In a previous study, ABAQUS/Explicit [12] was used to develop the numerical simulations. The three constuent materials include a woven glass-fibre/polypropylene matrix composite, a PVC foam and an adhesive. As they behave quite differently, different constitutive models and failure criteria are required to simulate their behaviour.

2.1 Modelling the woven glass fibre laminates

Prior to damage initiation, the woven glass fibre laminate has been modelled as an orthotropic elastic material. Damage initiation has been modelled using Hashin's failure criterion [13]. This criterion employs four damage initiation mechanisms, namely fibre tension, fibre compression, matrix tension and matrix compression. The criterion is established based on the relationship between the longitudinal, transverse and shear effective stress tensor components and the corresponding ultimate stresses within the plane of the composite.

The damage elastic matrix can be expressed as

$$\boldsymbol{C_d} = \frac{1}{D}\begin{bmatrix} (1-d_f)E_1 & (1-d_f)(1-d_m)\nu_{21}E_1 & 0 \\ (1-d_f)(1-d_m)\nu_{12}E_2 & (1-d_m)E_2 & 0 \\ 0 & 0 & (1-d_s)GD \end{bmatrix} \tag{4}$$

which relates stress and strain and where G is the shear modulus and D is an overall damage variable. In the above equation, d_f reflects the current state of fibre damage, d_m characterizes the current state of matrix damage, and d_s reflects the current state of shear damage. Using the longitudinal, transverse and shear effective stress tensor components within the plane of the GFRP, the damage initiation criteria can be determined [14, 15]. The longitudinal and transverse tensile and compressive fracture energies are required to control damage evolution.

2.2 The PVC foam

The foam under compression can be modelled as a crushable foam material for which the hardening curve was determined from a foam compression test. Deshpande and Fleck [16] proposed a phenomenological yield surface for these closed-cell foams as given by:

$$\varphi \equiv \frac{1}{\left[1+\left(\frac{\alpha}{3}\right)^2\right]}\left[\bar{\sigma}^2+\alpha^2\sigma_m^2\right]-\sigma_y^2 \le 0 \tag{5}$$

where σ_y is the uniaxial tensile or compressive yield strength of the foam, σ_m is the mean stress. The parameter α defines the shape of the yield surface, which is given by

$$\alpha = \frac{3k}{\sqrt{(3k_t + k)(3-k)}} \tag{6}$$

where k and k_t are related to the ratios of the initial uniaxial yield stress σ_c^o and the hydrostatic tensile yield stress p_t to the hydrostatic compressive yield stress p_c^o, respectively. The yield stress p_c in hydrostatic compression provides the evolution of the yield surface size and can be experssed as:

$$p_c(\varepsilon_{pl}^{vol}) = \frac{\sigma_c(\varepsilon_{pl}^{vol})\left[\sigma_c(\varepsilon_{pl}^{vol})\left(\frac{1}{\alpha^2}+\frac{1}{9}\right)+\frac{p_t}{3}\right]}{p_t + \frac{\sigma_c(\varepsilon_{pl}^{vol})}{3}} \tag{7}$$

where ε_{pl}^{vol} is the plastic volumetric strain for the volumetric hardening model which is equal to ε_{pl}^{axial} uniaxial compressive plastic strain. Therefore, p_c needs to be calculated based on the experimental data under the unaxial compressive test of the foam.

The rate-dependent behaviour of the PVC foam can be assumed to follow the relationships shown in Eq. (8). Damage initiation in a PVC foam can be modelled by applying the ductile damage criterion in conjunction with share damage criterion [12]. Both the damage evolutions of ductile and share failure are controlled by fracture energy in terms of the energy required for failure development.

$$\bar{\sigma}\left(\bar{\varepsilon}_{pl}, \dot{\bar{\varepsilon}}_{pl}\right) = \sigma_y\left(\bar{\varepsilon}_{pl}\right) R\left(\dot{\bar{\varepsilon}}_{pl}\right) \tag{8}$$

where $\bar{\varepsilon}_{pl}$ and R are the equivalent plastic strain and a stress ratio (= $\bar{\sigma}/\sigma_y$), respectively.

2.3 The resin layer and other contact conditions

A cohesive element, defined in terms of traction-separation, can be used to mesh the adhesive layer for modelling interaction between the GFRP layer and the PVC core. The traction-separation model in ABAQUS [12] assumes an initially linear elastic behaviour followed by initiation and development of damage. Damage development is controlled by the critical displacement to which the foam could be stretched prior to failure.

2.4 Typical numerical modelling results

Typical impact load-displacement traces of 4, 8 and 16 ply glass fibre laminates clamped in the square metal support are shown in Figure 8. An examination of the figure indicates that the FE analysis predicts the measured response reasonably accurately. The initial stiffnesses of the three laminates are close to the experimental responses and the peak loads of the 8 and 16 ply laminates are slightly over-estimated. The penetration and perforation response (i.e. After peak load) are simulated reasonably well, although the FE model predicts a sharp drop in load after peak load in the thickest laminate that is not observed experimentally.

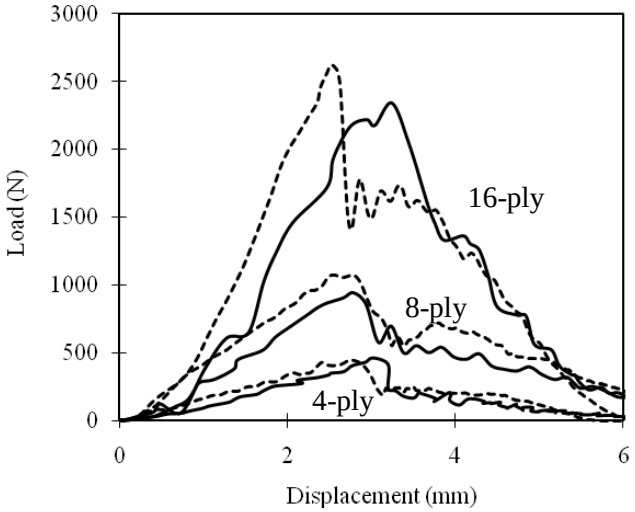

Figure 8. Impact load-displacement traces for the 4, 8 and 16-ply glass fibre laminates. The solid lines indicate experimental data and the dashed lines indicate the FE results [15].

The influence of varying projectile diameter on the impact response of the GFRP is summarised in the load displacement traces shown in Figure 9, which indicates that the model captures the essential features of the experimental data. Here, all four experimental traces exhibit similar trends with the force rising to a maximum before dropping sharply as the rear surface fibers fracture and the projectile begins to perforate the target. Clearly, increasing the projectile diameter results in an increase in the maximum impact force with the maximum force doubling over the range of diameters considered here.

Figure 10 shows comparisons between the FE and experimental load-displacement traces following low velocity impact on sandwich structures based on the three crossslinked foams. The correlation is good, with the model capturing most of the features in the experimental data. The FE model fails to identify the first peak, although the remainder of the trace is accurately predicted. Interestingly, the failure processes were similar in all of the sandwich structures, with the projectile shearing a relatively clean hole through the target, Figure 10(b).

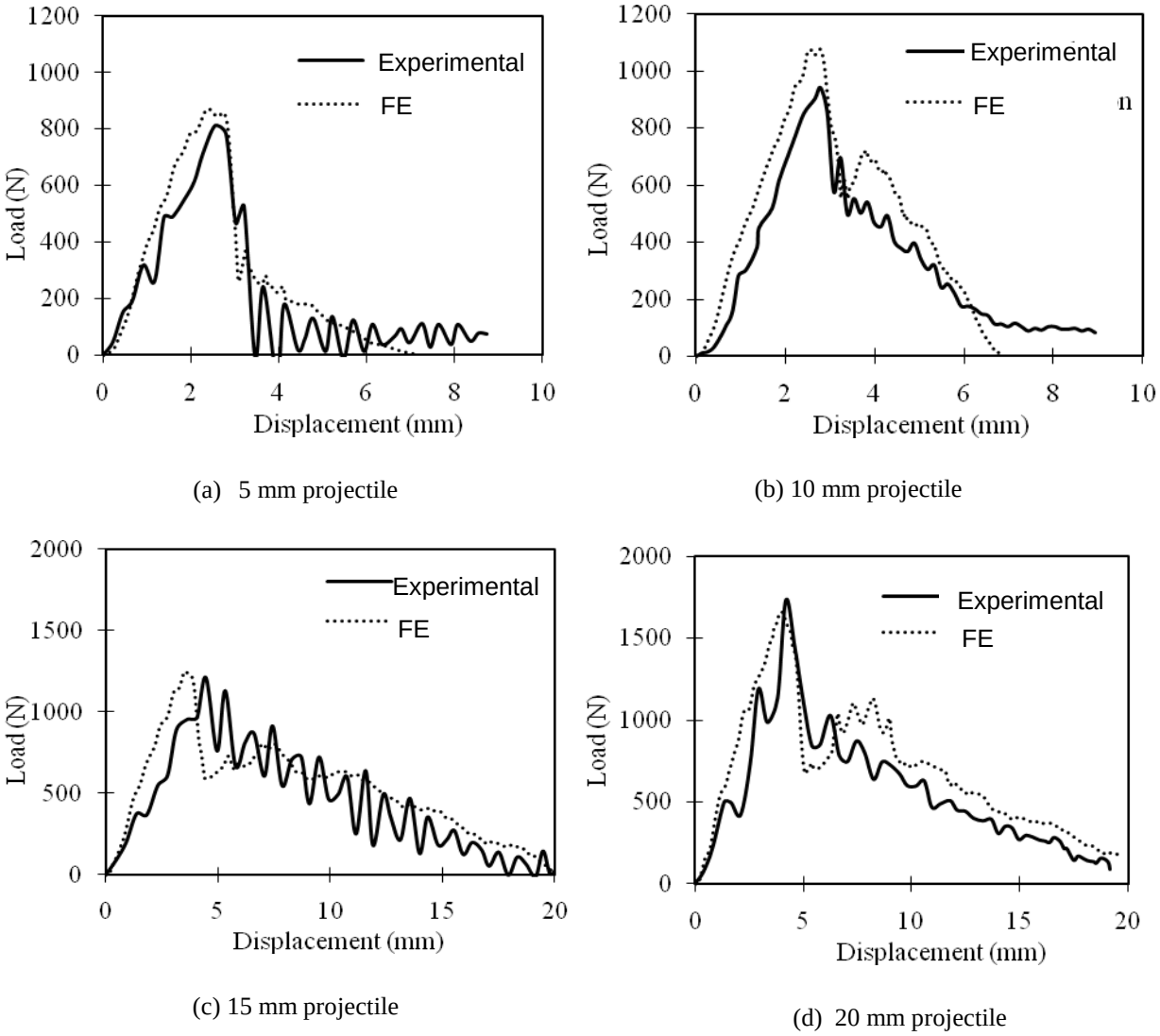

(a) 5 mm projectile

(b) 10 mm projectile

(c) 15 mm projectile

(d) 20 mm projectile

Figure 9. Load-displacement traces for the 8-ply glass fiber laminate impacted by projectiles of various diameters [15].

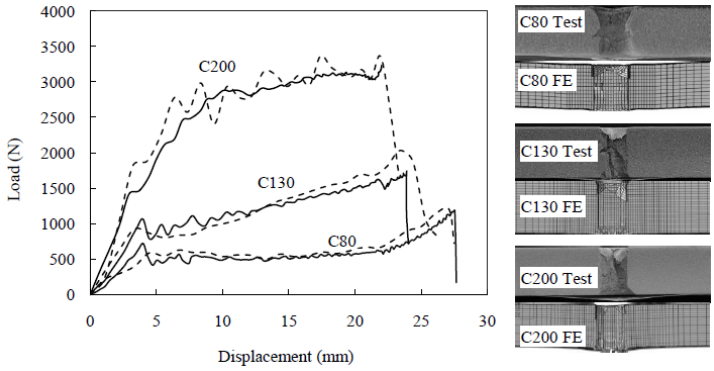

(a) load-displacement traces

(b) cross-sections

Figure 10. Comparison of load-displacement traces and cross-sections of sandwiches made with C80, C130 and C200 foam cores. The solid lines correspond to the experimental data and the dashed lines to the predictions [17].

Using validated models, perforation with angle of obliquity for sandwich panels based on two crosslinked PVC cores and a PET foam are simulated. Figure 11 shows the corresponding load-displacement traces. The impact angle refers to the angle between the axis of the projectile and the normal to the panel. From the figure, it is evident that the perforation energy increases with impact angle, for example, passing from approximately 29 Joules for a normal impact to approximately 35 Joules for thirty degree loading. Figure 11b also includes the cross-sections resulting from the FE predictions for impact at an angle of 30 degrees. The two crosslinked foams again exhibit a clear cylindrical-shaped perforation zone, similar to that observed under normal impact, so does the PET foam.

Impact tests on sandwich panels supported on water are also modelled. Figure 12 shows load-displacement traces for the L140 sandwich structure. Included in each figure are the

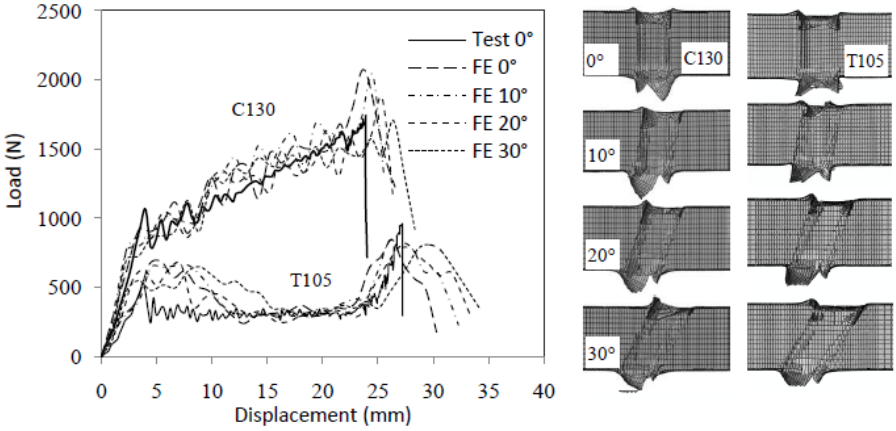

(a) load-displacement traces (b) C130 and T105 cross-sections

Figure 11. Load-displacement traces and cross sections of sandwich panels made with C70.130 cross-linked PVC and PET 92.105 PVC core subjected to oblique impact at incident angles of 10°, 20° and 30° [17].

associated FE predictions and the corresponding experimental trace for the previous impact tests (i.e. in the absence of water). It is clear that the rear surface peak is much higher in the fully supported wet panel than in its dry counterpart. In addition, the wet panel exhibits virtually no out of plane deflection, in contrast to the relatively flexible dry panel. The FE model predicts the experimental data with some success, although the final drop in force is not as abrupt.

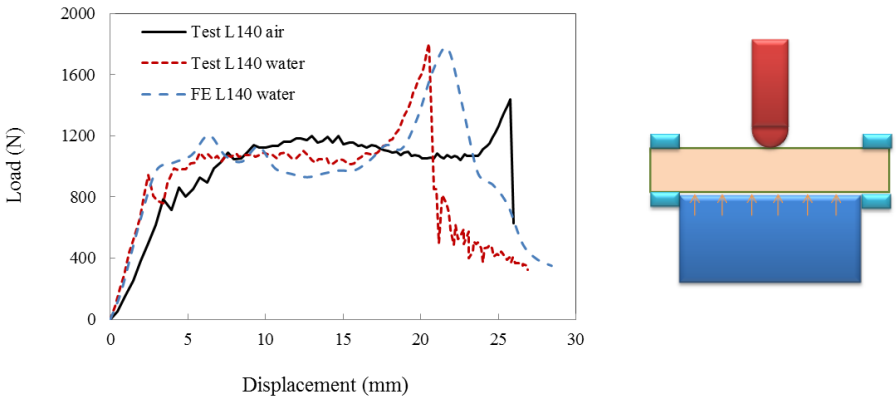

Figure 12. Comparison of load-displacement traces of sandwiches made with L140 foam cores between sandwiches supported on water and without support [17].

Graded foam core sandwich structures are also modelled. As an example, the force-displacement traces and failure modes for the L60/P60/L140 sandwich structure are exhibited in Figure 13. Clearly, the perforation force increasing in three steps between the peaks associated with fracturing the upper and lower shins. Moreover, the plateau force resulting from the fracture of the tough L140 foam is significantly higher than that requested to perforate its lower density L60 counterpart. The correlation between the test and FE modeling is good.

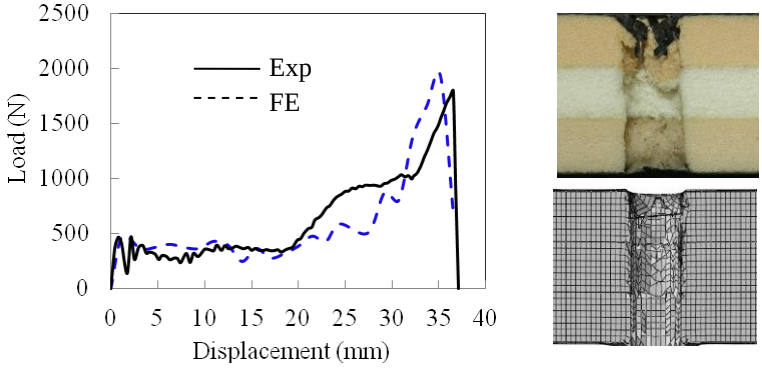

Figure 13. Load-displacement traces and resulting cross-sections for the L60/P60/L140 sandwich structure [18].

In order to investigate the influence of impact in a differential pressure environment on the dynamic response of a sandwich structure, low velocity impact simulations were undertaken on panels subjected to an air-pressure difference between their front and rear faces. The rear and the front faces were under pressures equivalent to atmospheric pressure at sea level and 10000 m, respectively. Figure 14 shows the predicted load-displacement traces for the two crosslinked foam sandwich structures. Included in the figure are the associated FE predictions for the sandwich structures impacted at the sea level (i.e. without an air-pressure differential) and in an air-pressure differential at an attitude of 10000 m, respectively. Figure 14 indicates that the higher density panels exhibit reasonably similar traces up to the point at which the projectile approaches the rear surface, followed by a notably higher second peak (broken line). However, the initial stiffness for the sandwich panel with the lower density foam core (C80) is enhanced, associated with a clear increase in the first peak load due to the higher support from a cabin pressure on the rear face (broken line).

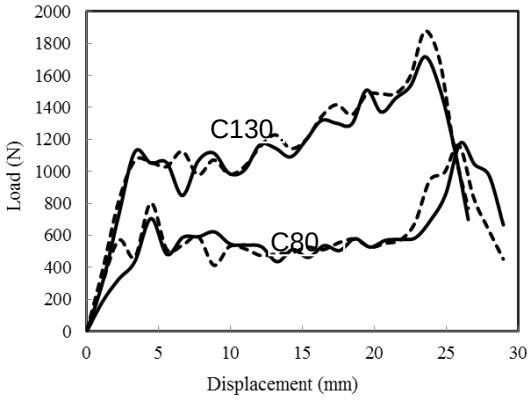

Figure 14. Comparison of the predicted load-displacement traces of cross-linked foam sandwich structures. The solid lines (validated) correspond to sea level conditions and the dashed lines (predicted) correspond to conditions at 10000 m [19].

References

[1] W.J. Cantwell. Geometrical effects in the low velocity impact response of GFRP. *Comp. Sci. and Tech*., volume (67): 1900-1908, 2007.
[2] P. Sjoblom. Simple design approach against low velocity impact damage. *Proc. 32nd SAMPE Symp. Anaheim*, 529-539, 1987.
[3] L.S. Sutherland and C. Guedes Soares. Contact indentation of marine composites. *Comp. Struct*., volume (70): 287-294, 2005.
[4] G. Zhou. Prediction of impact damage thresholds of glass fibre reinforced laminates. *Comp. Struct*., volume (31): 185-193, 1995.
[5] G.A.O. Davies and X. Zhang. Impact damage prediction in carbon composite structures. *Int. J. of Impact Eng*., volume (16): 149-170, 1995.
[6] G.A. Schoeppner and S. Abrate. Delamination threshold loads for low velocity impact on composite laminates. *Comp. Part A: Appl. Sci. Man*., volume (31): 903–915, 2000.
[7] F.J. Yang and W.J. Cantwell. Impact damage initiation in composite materials. *Comp. Sci. and Tech*., volume (70): 336-342, 2010.
[8] G.A.O. Davies, X. Zhang. Impact damage prediction in carbon composite structures. *Int J Impact Eng.*, volume (16): 149–70, 1995.
[9] Zhou G. Prediction of impact damage thresholds of glass fibre reinforced laminates. *Compos. Struct.*, volume (31): 185–93,1995.
[10] M.Z. Hassan and W.J Cantwell. The Influence of Core Properties on the Perforation Resistance of Sandwich Structures - An Experimental Study. *Comp. Part B*, volume (43): 3231-3238, 2012.
[11] M.S. Hoo Fatt and K.S. Park. Dynamic models for low velocity impact damage of composite sandwich panels - Part B: Damage initiation. *Comp. Struct*., volume (52): 353-364, 2001.
[12] ABAQUS/Explicit, User's Manual, Version 6.9, Hibbitt, Karlsson & Sorensen, Inc., 2009.
[13] Z. Hashin. Failure Criteria for Unidirectional Fiber Composites. *Journal of Applied Mechanics*, volume (47): 329–334, 1980.
[14] J. Fan, Z.W. Guan and W.J. Cantwell. Numerical modelling of perforation failure in fibre metal laminates subjected to low velocity impact loading. *Composite Structures*, volume (93): 2430–2436, 2011.
[15] J. Fan, Z.W. Guan and W.J. Cantwell. Modelling perforation in glass fiber reinforced composites subjected to low velocity impact loading. *Polymer Composites*, volume 32(9): 1380-1388, 2011.
[16] V.S. Deshpande and N.A. Fleck. Multi-axial yield behaviour of polymer foams. *Acta Materialia*, volume (49): 1859-1866, 2001.
[17] J. Zhou, M.Z. Hassan, Z.W. Guan and W.J. Cantwell. The low velocity impact response of foam-based sandwich panels. *Composites Science and Technology*, volume 72(14): 1781-1790, 2012.
[18] J. Zhou, M.Z. Hassan, Z.W. Guan and W.J. Cantwell. The Impact Response of Graded Foam Sandwich Structures. *Composite Structures*, volume (97): 370-377, 2013.
[19] J. Zhou, M.Z. Hassan, Z.W. Guan and W.J. Cantwell. The perforation resistance of sandwich structures subjected to low velocity projectile impact loading. *Aeronautical Journal*, volume 116 (1186): 1247-1262, 2012.